Unveiling the membrane bound dihydroorotate: Quinone oxidoreductase from *Staphylococcus aureus*

Filipe M. Sousa [a,b], Patrícia Pires [b], Andreia Barreto [b], Patrícia N. Refojo [a], Micael S. Silva [c], Pedro B. Fernandes [a], Ana P. Carapeto [b,d], Tiago T. Robalo [b,d], Mário S. Rodrigues [b,d], Mariana G. Pinho [a], Eurico J. Cabrita [c], Manuela M. Pereira [a,b,*]

[a] *Instituto de Tecnologia Química e Biológica – António Xavier, Universidade Nova de Lisboa, Av. da República EAN, 2780-157 Oeiras, Portugal*
[b] *University of Lisbon, Faculty of Sciences, BioISI - Biosystems & Integrative Sciences Institute, Campo Grande, C8, 1749-016 Lisboa, Portugal*
[c] *UCIBIO, Departamento de Química, Faculdade de Ciências e Tecnologia, Universidade Nova de Lisboa, 2829-516 Caparica, Portugal*
[d] *Departamento de Física, Faculdade de Ciências, Universidade de Lisboa, 1749-016 Lisboa, Portugal*

ARTICLE INFO

ABSTRACT

Staphylococcus aureus is an opportunistic pathogen and one of the most frequent causes for community acquired and nosocomial bacterial infections. Even so, its energy metabolism is still under explored and its respiratory enzymes have been vastly overlooked. In this work, we unveil the dihydroorotate:quinone oxidoreductase (DHOQO) from *S. aureus*, the first example of a DHOQO from a Gram-positive organism. This protein was shown to be a FMN containing menaquinone reducing enzyme, presenting a Michaelis-Menten behaviour towards the two substrates, which was inhibited by Brequinar, Leflunomide, Lapachol, HQNO, Atovaquone and TFFA with different degrees of effectiveness. Deletion of the DHOQO coding gene (*Δdhoqo*) led to lower bacterial growth rates, and effected in cell morphology and metabolism, most importantly in the pyrimidine biosynthesis, here systematized for *S. aureus* MW2 for the first time. This work unveils the existence of a functional DHOQO in the respiratory chain of the pathogenic bacterium *S. aureus*, enlarging the understanding of its energy metabolism.

1. Introduction

Staphylococcus aureus (*S. aureus*) is a Gram-positive pathogenic bacterium responsible for both hospital and community-acquired infections which can lead to relatively minor skin lesions or, in more serious cases, to life threatening diseases, such as bacteremia, endocarditis or hemolytic pneumonia [1]. *S. aureus* infections are most dangerous when caused by methicillin-resistant strains (MRSA), which are one of the leading causes of nosocomial infections worldwide [2,3]. *S. aureus* shows a great ability to adapt to diverse environmental conditions, especially during host colonization, which makes this bacterium an exceptional opportunistic pathogen. The adaptability of this pathogen comes from its metabolic versatility, which in part is due to the relatively complex composition of its respiratory chain.

S. aureus is a facultative anaerobic bacterium, able to respire or ferment [4]. When respiring it can reduce nitrate or oxygen by using either a nitrate reductase [5] or its oxygen reductases [6], respectively.

These enzymes are quinol oxidases and determine the type of respiration being used, aerobic or anaerobic. However, the ability to use several substrates for the reduction of the quinone pool is what gives this organism its metabolic plasticity. *S. aureus* contains a vast array of quinone reductases which connect the different metabolic pathways to the respiratory chain. Our bioinformatic studies have suggested the existence of genes coding for a glycerol-3-phosphate:quinone oxidoreductase (G3PQO), a succinate:quinone oxidoreductase (SDH), a formate:quinone oxidoreductase (Fdn—N), a malate:quinone oxidoreductase (MQO) and a dihydroorotate:quinone oxidoreductase (DHOQO) [7,8], in addition to four other enzymes have already been isolated and characterized: two NADH:quinone oxidoreductases (NDH-2 s) [9,10], a pyruvate:quinone oxidoreductase (PQO) [11] and a sulfide:quinone oxidoreductase (SQR) [12].

In this work we unveil the DHOQO from *S. aureus*. DHOQOs are flavin-containing monotopic enzymes, meaning they are attached to a single side of the lipid membrane, that catalyse the oxidation of

---

dihydroorotate (DHO) to orotate and concomitant reduction of a liposoluble quinone to quinol [13]. The use of quinones as substrates makes DHOQO directly involved in the respiratory chain. Moreover, by oxidizing DHO, they are also part of the so-called *de novo* pyrimidine biosynthesis. Because of this double role, DHOQOs have been regarded as possible therapeutic targets for treatment of cancer, immunological disorders and bacterial/viral infections [14–19].

Initially identified in 1964, the DHOQO from *Escherichia coli* was the first studied example of a class 2 - quinone reducing - dihydroorotate dehydrogenase [20]. Since then, DHOQOs from more than ten different species have been successfully isolated and characterized [21–31] from which only three belong to bacteria (*E. coli, Helicobacter pylori* and *Mycobacterium tuberculosis*). The crystallographic structures of seven different DHOQOs were already solved: *Homo sapiens* [32–38], *Plasmodium falciparum* [27,39–42], *Rattus norvegicus* [25], *Schistosoma mansoni* [26], *E. coli* [43], *Helicobacter pylori* (PDB ID: 6B8S) and *Mycobacterium tuberculosis* (PDB ID: 4XQ6). Much due to the existing sample of studied enzymes, DHOQOs were considered to be present exclusively in Eukaryotes and Gram-negative bacteria. Recently we performed a bioinformatic study systematizing the presence of DHOQOs across the phyla of life and proposed that these enzymes were also present in Gram-positive bacteria [44], but this had yet to be experimentally confirmed.

In this work we explored *S. aureus* DHOQO both from a molecular and a cellular perspective. This knowledge will contribute to the fundamental understanding of *S. aureus*' energy and pyrimidine synthesis metabolisms.

2. Materials and methods

2.1. Gene expression, protein purification and biochemical characterization

Escherichia coli Rosetta 2 (DE3) pLysS cells were transformed, using the heat shock method, with the plasmid pET-28a (+) containing the *S. aureus* DHOQO coding gene (Gene ID 3921361). Cells were grown in 2YT medium at 37 °C and 180 rpm, supplemented with 100 μg/mL kanamycin and 34 μg/mL chloramphenicol. Expression was induced by adding 1 mM IPTG (isopropyl-β-D-1-thiogalactopyranoside) when cells reached an OD_{600nm} of 0.6. Cells were harvested 4 h after induction, immediately resuspended in 100 mM K_2HPO_4/KH_2PO_4 pH 7.0, 250 mM NaCl, and disrupted in a French press at 40 MPa. Soluble and membrane fractions were separated by ultracentrifugation at 200,000 *g* for 2 h. The obtained membrane pellet was resuspended in 100 mM $K_2HPO_4/$ KH_2PO_4 pH 7.0, 2 M NaCl using a Potter-Elvehjem homogenizer and incubated overnight at 4 °C. The obtained resuspended fraction was again subjected to ultracentrifugation at 200,000 *g* for 1 h and resuspended in 100 mM K_2HPO_4/KH_2PO_4 pH 7.0, 10 % glycerol, 250 mM NaCl, before the chromatographic procedures. Chromatographic steps were performed on an AKTA Prime Plus system (GE Healthcare) using a His-Trap HP 5 mL column (GE Healthcare). Protein was eluted with a histidine gradient (0 to 250 mM), in the same buffer used to resuspend the injected sample. The purified protein was analysed by mass spectrometry at the MS Unit, ITQB/IBET (using a positive reflector MS and MS/MS modes in a 4800 plus MALDI-TOF/TOF mass spectrometer and the 4000 Series Explorer Software v.3.5.3) and stored at −80 °C until needed. Protein purity was analysed by SDS-PAGE using a Mini-PROTEAN® Electrophoresis System from BIORAD and UV–Visible spectroscopy (Abs_{280nm}/Abs_{450nm} ratio) using a Shimadzu UV-1900. The flavin prosthetic group was identified by reverse phase chromatography. The flavin was obtained by centrifugation of the denatured protein, which was incubated at 100 °C for 10 min. The supernatant was injected in a C18 column operated in a Waters-Alliance HPLC system. The column was equilibrated with 5 mM ammonium sulphate and the sample was eluted at 1 mL/min with an isocratic gradient from 10 to 80 % of a 5 % methanol solution. Commercial FAD (Merck) and FMN (Sigma Aldrich) were used as standards. To investigate the oligomerization state

of the enzyme a Native PAGE was performed using 0.5 μg of the purified enzyme and high molecular mass markers. The thermal stability of the enzyme was investigated by a thermal denaturation assay (25–90 °C) following the fluorescence emission at 530 nm by exciting the flavin at 450 nm. 2 μM of purified DHOQO in 100 mM K_2HPO_4/KH_2PO_4 pH 7.0, 250 mM NaCl buffer was used.

2.2. Structural modelling

To illustrate and understand the discussed structural features of *S. aureus* DHOQO, we built a three-dimensional homology model of this enzyme using Modeller9v15 [45]. The model was generated based on the available crystallographic structures of other DHOQOs (PDB ID 1F76 [43], 4XQ6, 6B8S, 4ORI [46], 6UY4 [26], 3SFK [47]). After the model was built, a full stereochemical validation using PROCHECK [48] was performed.

2.3. Kinetic studies

Steady-state kinetic assays were performed on a Shimadzu UV-1900 monitoring the formation of quinol by decreasing the absorbance at 270 nm at 37 °C with a fixed protein concentration of 150 nM. pH values between 5.5 and 9 were tested using 50 mM MES, 50 mM Bis-Tris Propane, 250 mM NaCl buffer. Kinetic parameters (V_{max} and K_M) for the two substrates were calculated at pH 7.5, using the Michaelis-Menten model. DMN was dissolved in DMSO and added to the reaction mixture prior to the start of the reaction (which was achieved by addition of protein). In this way, problems with determination of the Km can be ruled out. Inhibition studies were performed for 2-heptyl-4-quinolinol 1-oxide (HQNO, Enzo Life Sciences), thenoyltrifluoroacetone (TTFA, Sigma-Aldrich), Atovaquone (Tokyo Chemical Industry), Brequinar (Cayman Chemical Company), Leflunomide (Santa Cruz Biotechnology), and Lapachol (Santa Cruz Biotechnology), all dissolved in DMSO, similarly to DMN, in the same conditions as those described above. The DMSO concentration in the final reaction mixture was kept at 5 %. The half-maximal inhibitory concentration (IC_{50}) parameter was determined using the model equation: % activity = V_{min} + [(V_{min} - V_{max}) / ($10^{\log [I] - \log [IC50]}$)]; with [I] being the inhibitor concentration. DMN (electron acceptor) was synthesized from menadione from Sigma Aldrich as described elsewhere [49] and DHO (electron donor) was acquired from Sigma Aldrich.

2.4. Protein-substrate interaction studies

Fluorescence quenching studies were performed to obtain the dissociation constants (K_D) for the different interacting molecules. Fluorescence emission spectra were obtained at 25 °C using a Jobin Yvon HORIBA spectrofluorometer, exciting the samples at 295 nm. The reduction in emission at 350 nm was normalized (% ΔF) and plotted *versus* the substrate concentration. K_D values were calculated using Monod-Wyman-Changeux (MWC) model equation for DHO, 1,4-dimethyl-menaquinone (DMN), 2,3,5,6-Tetramethyl-1,4-benzoquinone (DUR), HQNO, DHO in the presence of HQNO and DMN in the presence of HQNO.

2.5. S. aureus strains and bacterial growth conditions

All the strains and plasmids used in this study are listed in Tables S1 and S2 in supplemental material. The sequences of the primers used are listed in Table S3.

S. aureus strains were grown on TSA or in TSB supplemented with erythromycin (10 μg/mL) when needed at 37 °C with aeration. Overnight cultures of *S. aureus* MW2 strains were diluted to OD_{600nm} = 0.05 in TSB (VWR) and grown at 37 °C for 11 h with OD_{600nm} and pH measurements taken every 1.5 h. *E. coli* DC10B cells were grown on LA or LB supplemented with erythromycin (10 μg/mL).

For NMR-based metabolomic analyses, 1.5 mL samples were collected by centrifugation at different time-points during the growth, and the supernatant and pellet were stored at −20 °C. NMR-based metabolomic analysis was performed for 3 conditions: *S. aureus* MW2 (WT strain) and *S. aureus* MW2 with *dhoqo* gene knocked-out (Δ*dhoqo* strain) grown in TSB medium or in TSB medium supplemented with 100 μM uracil (Δ*dhoqo* + U).

The handling of *S. aureus* and *E. coli* strains was performed inside a laminar flow chamber (NinoLaf Safety Cabinet, Modell ninoSAFE 1200).

2.6. Construction of S. aureus dhoqo knockout mutants

The Δ*dhoqo* mutant was constructed using the pMAD vector [50] containing the upstream and downstream regions of the gene of interest. The upstream and downstream regions of *dhoqo* gene were amplified by PCR, using primers P1-DHOQO-KO and P2-DHOQO-KO, and P3-DHOQO-KO and P4-DHOQO-KO, respectively (Table S3). An overlap PCR, using the pair of primers P1-DHOQO-KO and P4-DHOQO-KO, was performed to join the PCR fragments encoding the upstream and downstream regions. The resulting fragment was then digested with *Xma*I and *Mlu*I (NEB) and inserted into the pMAD vector (digested with the same enzymes). The insertion was confirmed by PCR and sequencing. Recombination and integration of the plasmid into the chromosome was obtained after a two-step homologous recombination process as previously described [50]. Briefly, the pMAD_Δ*dhoqo* vector was electroporated into *S. aureus* RN4220 strain (grown at 30 °C, in TSA, erythromycin and X-gal) and transduced into *S. aureus* MW2 using phage 80α. In the first step, recombinants were selected at a non-permissive temperature of 43 °C, using erythromycin and light blue colony colour. In the second step, cells were incubated at the permissive temperature of 30 °C in the absence of antibiotic selection, and white, erythromycin sensitive colonies in which the vector had been excised were selected. Gene deletions were confirmed by PCR and sequencing of the amplified fragment.

2.7. Construction of promoter-GFP fusions

To construct a promoter-GFP fusion in *S. aureus*, a 700 bp fragment upstream of the *dhoqo* gene, containing the promoter region, was amplified by PCR using P1-PR_DHOQO-GFP and P2-PR_DHOQO-GFP. The *gfp* gene was amplified from pFast3 [51] by PCR using P3-PR_DHOQO-GFP and P4-PR_DHOQO-GFP. The two fragments were joined by overlap PCR using P1-PR_DHOQO-GFP and P4-PR_DHOQO-GFP. The resulting fragment was digested with *Eco*RI and *Xma*I and inserted into the integrative vector pSP64E [52], originating pSP64E-PR_dhoqo-GFP whose sequence was confirmed by PCR and sequencing analyses. The pSP64E-PR_dhoqo-GFP was then electroporated into *S. aureus* RN4220 and transduced to *S. aureus* MW2 cells using phage 80α. The correct integration was confirmed by PCR and sequencing analyses.

2.8. Fluorescence-activated cell sorting

S aureus WT and *S. aureus* dhoqo promoter:gfp growths were performed in TSB medium. Samples were collected every 1.5 h by centrifugation and stored at 4 °C for later analysis. Samples were diluted in filtered phosphate-buffer saline (PBS) solution to an OD_{600nm} of 0.5 and were analysed in an S3e cell sorter (Bio-Rad). The fluorescence of 10,000 single cells was measured using a 488 nm laser. Fluorescence intensity is presented by subtracting background fluorescence of WT to that of cells containing the promoter fusion *dhoqo* promotor::GFP.

2.9. NMR based metabolomics

All samples for NMR experiments were prepared in 200 mM sodium phosphate, 10 % (v/v) D_2O, and 0.5 mM sodium-2,2-dimethyl-2-silapentane-5-sulfonate-d6 (DSS, Eurisotop), pH 7.0 ± 0.1 (pH was adjusted with negligible microliter addition of HCl or NaOH solutions) and measured with a Docu-pH meter (Sartorius) calibrated with standard solutions. Typically for each aliquot (450 μL) from *S. aureus* medium, 50 μL of 2 M sodium phosphate (pH ≈ 6.6) and 5 mM DSS in D_2O were added. The final solution (500 μL) was transferred to a 5 mm NMR tube. Triplicates for each growth time-point (0, 1.5, 3, 4.5, 6, 7.5 and 9 h) were performed for every growth condition (*WT*, Δ*dhoqo* and Δ*dhoqo* + U).

All NMR spectra were collected at 298.2 K on a 500 MHz Bruker NEO spectrometer equipped with a 5 mm triple-resonance ^{1}H-optimized Prodigy N_2-cooled cryogenic probe head with z-gradients, operating at a ^{1}H Larmor frequency of 500.34 MHz. ^{1}H NMR spectra were recorded using a 1D NOESY (nuclear Overhauser effect spectroscopy) pulse sequence with pre-saturation for water signal suppression ("noesypr1d" in Bruker standard library), using a relaxation delay of 2 s and mixing time of 100 ms. Spectra were acquired with 65 K data points and 128 scans for a spectral width of 5882 Hz cantered at the water resonance frequency (2349.6 Hz). Data were processed and analysed using Bruker TopSpin4.0. All spectra were automatically phased and baseline was corrected.

Metabolites were identified in the spectra and their quantification was performed by integration of selected spectral resonances: the relative concentration of each metabolite was calculated in relation to the known concentration of the added DSS using the integrals of the corresponding resonance frequencies in the spectrum and the corresponding number of protons. The uncertainty in the concentration is the standard deviation of the mean from triplicate measurements.

2.10. Atomic force microscopy measurements

Cell samples were applied in a freshly prepared mica surface and were characterized by AFM with a PicoSPM LE (Molecular Imaging) system and Agilent Technologies PicoView 1.14.4 software (Keysight Technologies, Santa Rosa, CA, USA). Fresh mica surfaces were prepared by removal of the exposed layer using double-sided scotch-tape. The images were obtained in air, at room temperature, with HQ:NSC35/Hard/Al BS-C μmasch cantilevers with nominal cantilever stiffness of 5.4 N/m and nominal tip radius < 20 nm in dynamic mode. To measure cell surface roughness ~2 × 2 μm^2 images with 512 × 512 pixels were obtained. Cell height (in nanometers) refers to the maximum distance defined by a perpendicular vector between the mica plane and the cell surface. Cell diameter (in nanometers) is defined as the maximum distance between two cell limits in a parallel plane to the one defined by the mica surface.

3. Results and discussion

3.1. S. aureus' DHOQO biochemical characterization

The gene *mw2509*, also known as *pyrD*, from *S. aureus* MW2 is strictly conserved throughout all currently sequenced *S. aureus* strains. We successfully cloned and expressed *pyrD* and purified the produced 354 amino acid protein (UniProt ID: A0A0H3K1V6), assigned as a dihydroorotate dehydrogenase. The enzyme was heterologously produced with a His-Tag in *E. coli* Rosetta cells and purified using an affinity chromatography column (Fig. S1). The purified ~40 KDa protein showed a characteristic spectrum of a flavoprotein, with maxima around 375 and 450 nm (Fig. 1). Addition of dihydroorotate (DHO) to the purified enzyme (in a 1:1 ratio) readily leads to a decrease in the absorbance at the 300–500 nm region, corresponding to the reduction of the flavin. Exposure of the reduced enzyme to atmospheric O_2 results in its reoxidation and reversion of the spectral features.

The enzyme was purified in a monomeric conformation (Fig. S1) and was able to keep its structural conformation stable until approximately 45 °C (Fig. S3). The type of flavin cofactor was identified by reverse-
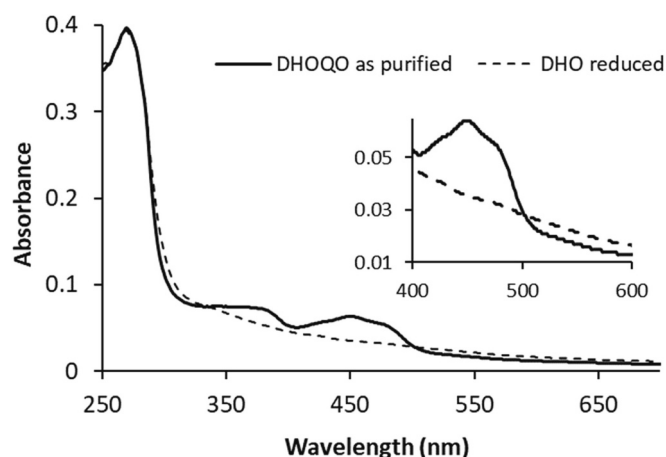
Fig. 1. UV–visible absorption spectra of DHOQO from *S. aureus* as purified (solid line) and reduced with dihydroorotate (dashed line). The inserted panel shows a zoomed section of the absorption spectra in the 400–600 nm region.

phase HPLC analysis as a flavin mononucleotide (FMN) (Fig. S2). The purified enzyme catalysed the electron transfer between DHO and quinone, allowing us to confirm that this protein is a dihydroorotate: quinone oxidoreductase (DHOQO).

Moreover, we observed that *S. aureus* DHOQO contains the hallmarks of its family of proteins [44]. The structural homology model of this protein (Fig. 2) shows the presence of a catalytic serine residue, S179, in the loop ahead of the DHO binding site (Fig. 2, panel A). We also noticed the presence of the residues belonging to the "SSPNT" catalytic motif [53] and of the two α-helices of the N-terminal domain [13] (Fig. 2, panel B). These two helices are considered key not only for membrane attachment but also for quinone interaction, as they harbour the "ExAH" motif (Fig. 2, panel B) previously proposed as part of a conserved quinone binding motif [44].

3.2. *S. aureus' DHOQO preferentially reduces menaquinone and is inhibited differently by different classes of inhibitors*

DHOQO uses a liposoluble quinone as its preferential electron acceptor. As for other monotopic quinone reductases, the type of quinone reduced in physiological conditions depends almost exclusively on its availability at the membrane, as most organisms produce a single type of quinone [54]. Quinone preference also depends on the stereochemistry of the binding site as proved by testing the enzymatic activity with both the physiological and a different type of quinone (menaquinone *vs* ubiquinone) [55]. In the case of *S. aureus*, the predominant quinone found on the lipid membrane is Menaquinone-7 [56]. Because of the low solubility of this molecule, we used a structural menaquinone analogue lacking the aliphatic carbon tail, dimethyl-naphthoquinone (DMN). The enzyme showed a Michaelis-Menten behaviour towards the two substrates (DMN and DHO), with a V_{max} of 12.9 ± 0.46 μmol^{-1} min^{-1} mg^{-1} (Fig. 3, panels A and B). The calculated K_M value was lower for DMN than for DHO (15.5 ± 0.7 and 72 ± 7 μM respectively). All activity measurements were performed at pH 7.5, which was determined to be the optimal pH of activity for this enzyme (Fig. 3, panel C).

The interaction of DHOQO with its two substrates was further characterized by fluorescence quenching studies, which allowed us to determine a dissociation constant (K_D) of 61 ± 4 and 55 ± 4 μM, for DHO and DMN respectively (Fig. 4). Crystallographic structures of DHOQO with bound DHO are available [43], which together with biochemical characterization data (both for DHOQOs and soluble dihydroorotate dehydrogenases) indicates how the electron donor binds to the protein. In contrast to DHO bound, to date there are no available DHOQO structures with a bound quinone, and because of that, the binding site of the electron acceptor is still a matter of discussion. It is

considered to be located at the N-terminal domain of the enzyme, close to the place where the membrane attachment occurs [57]. Considering what was observed for other monotopic quinone reductases [58–60], the two substrates were shown to bind at different locations (*i.e.*, in opposite sides of the isoalloxazine ring of the flavin), we raised the hypothesis that this may also occur in the case of DHOQOs. To test this hypothesis, we performed additional fluorescence quenching studies, but this time HQNO was included in the titration mixture, both when titrating with DHO or with the quinone. HQNO is a quinone analogue known to inhibit other quinone reductases at the quinone binding site [61]. HQNO was first shown to interact (Fig. S4, panel B) and to inhibit DHOQO from *S. aureus* (see below). The presence of HQNO while titrating DHOQO with DHO showed no effect, suggesting HQNO and DHO bind at different sites. However, when titrating DHOQO with DMN, HQNO was shown to strongly interfere with DMN binding, affecting not only the calculated binding constant (now 259 ± 13 μM) but also altering the maximum quenching effect observed (from 78 % to 45 %). These results confirm that DHO and DMN bind at different sites of DHOQO (*re*- and *si*-side of the flavin, respectively) and that HQNO interferes with quinone binding. Fluorescence quenching studies also allowed to observe the preference of DHOQO for menaquinone over ubiquinone, as the respective determined K_D were 158 ± 8 and 55 ± 4 μM for duroquinone and DMN (Fig. S4, panel A), confirming a tighter binding for DMN. HQNO K_D was also measured using the same approach and determined to be 32 ± 13 μM (Fig. S4, panel B), lower than that for any of the tested quinones.

More than a quinone reductase inhibitor, HQNO is also known as an anti-staphylococcal agent. During host colonization, *S. aureus* often interacts with other bacteria, specifically *Pseudomonas aeruginosa*. This organism is known to produce HQNO, hampering staphylococcal growth by inhibiting the respiratory chain during competitive colonization [62,63]. Investigating HQNO inhibition of *S. aureus* DHOQO further contributes to a better understanding of the mechanisms underlying microbial interaction. HQNO is here shown for the first time to inhibit the activity of DHOQO with a calculated IC$_{50}$ of 0.68 ± 0.05 μM (Fig. 5). Contrarily to HQNO, other classes of inhibitors have long been shown to hamper the activity of other DHOQOs. Some of the most relevant inhibitors observed to act on this family of enzymes are Leflunomide, Brequinar, Atovaquone and Lapachol [64]. Molecules with an inhibitory effect on DHOQOs have been proposed as possible therapeutical strategies for rheumatoid arthritis [65,66], neuroblastoma [67], COVID-19 [68], influenza virus [69], malaria [70], among others, but not for *S. aureus* associated infections. For this reason, we performed an exploratory inhibitory study on *S. aureus* DHOQO, covering different classes of inhibitors and a broad chemical universe (Fig. 5).

We determined the IC$_{50}$ of the previously mentioned inhibitors plus TTFA, which has been shown to interact with the quinone binding site of succinate:quinone oxidoreductase and to inhibit its activity [71,72]. The obtained results showed that Atovaquone was the least efficient of the six tested molecules, with a IC$_{50}$ of at least 740 ± 125 μM. However, this result must be taken with caution, as the inhibitor concentrations used (limited by Atovaquone's solubility) lead to a very slight inhibitory effect. The remaining five molecules, including HQNO, all significantly inhibited DHOQO's activity and their calculated IC$_{50}$ were 50 ± 9 μM for Brequinar, 157 ± 11 μM for Leflunomide, 33 ± 8 μM for Lapachol and 228 ± 9 μM for TTFA. The most significant differences, when comparing to the inhibition studies using the human DHOQO, were observed for Brequinar and Lapachol. The former was observed to be the most efficient of the tested inhibitors for the human enzyme (with a IC$_{50}$ of 0.007 μM) and the latter provided a more impactful inhibitory effect than Brequinar, in the case of the enzyme from *S. aureus*. From the six studied inhibitors, the one with the lowest IC$_{50}$ was HQNO. One of the reasons that may have contributed to this result is the fact that HQNO is the only molecule with an aliphatic carbon tail, which may help in an efficient binding at the quinone binding site. A summary table of the determined IC$_{50}$, as well as the IC$_{50}$ found in the literature, is given in Table 1.
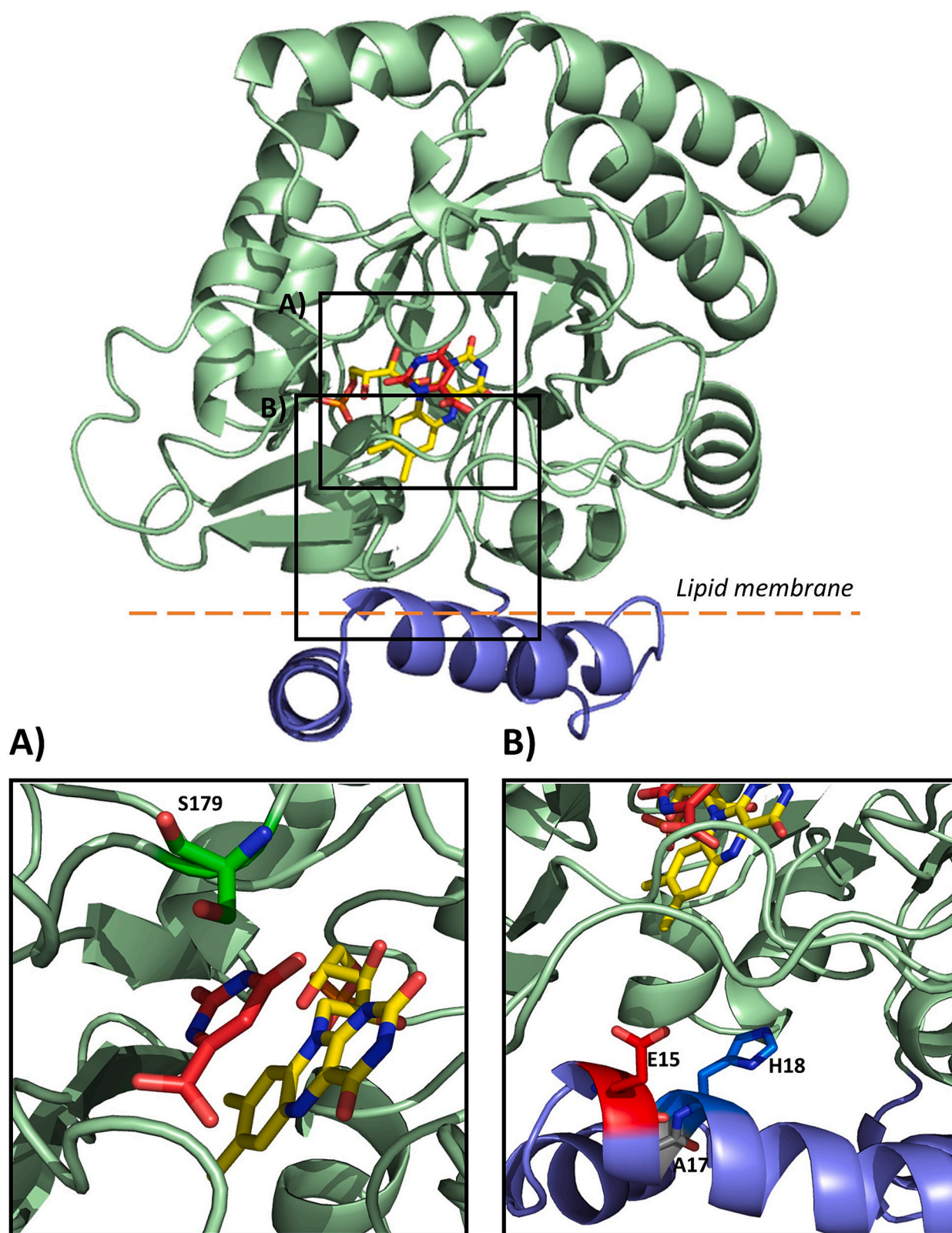
Fig. 2. Cartoon representing the homology model structure of DHOQO from *S. aureus* (pale green and blue). The N-terminal domain is highlighted in dark blue. Panel "A" points out the DHO (red sticks) binding site, close to FMN (yellow sticks) and the catalytic base (green sticks). Panel "B" highlights the "ExAH" motif of the quinone binding site. DHO binding location was estimated by superimposition with the available DHO bound structures. The homology model was obtained as described in material and methods section.
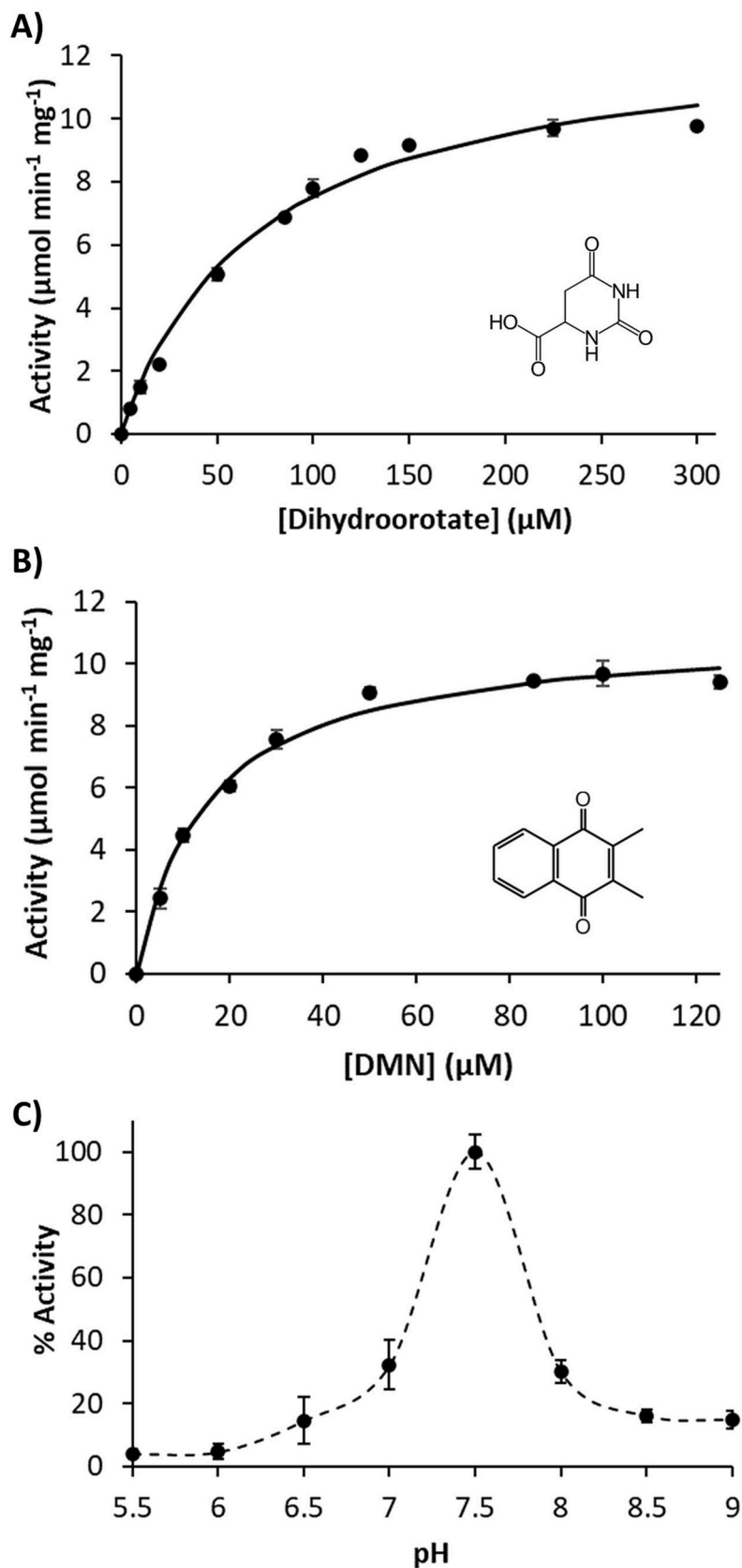
Fig. 3. Steady-state kinetic analyses of the DHOQO from *S. aureus*. Panel "A" shows enzyme activity with different DHO concentrations (from 0 to 300 μM) in the presence of a constant concentration of DMN (125 μM) and panel "B" presents enzyme activity with different concentrations of DMN (from 0 to 125 μM) in the presence of a constant concentration of DHO (150 μM). Panel "C" shows the relative enzymatic activity (% activity) measured within a range of pH between 5.5 and 9. All points result from three experimental measures and error bars represent the standard deviation of such triplicates. Enzymatic activity quantified quinol formation (μmol/min/mg) by measuring the absorbance variation at 270 nm.
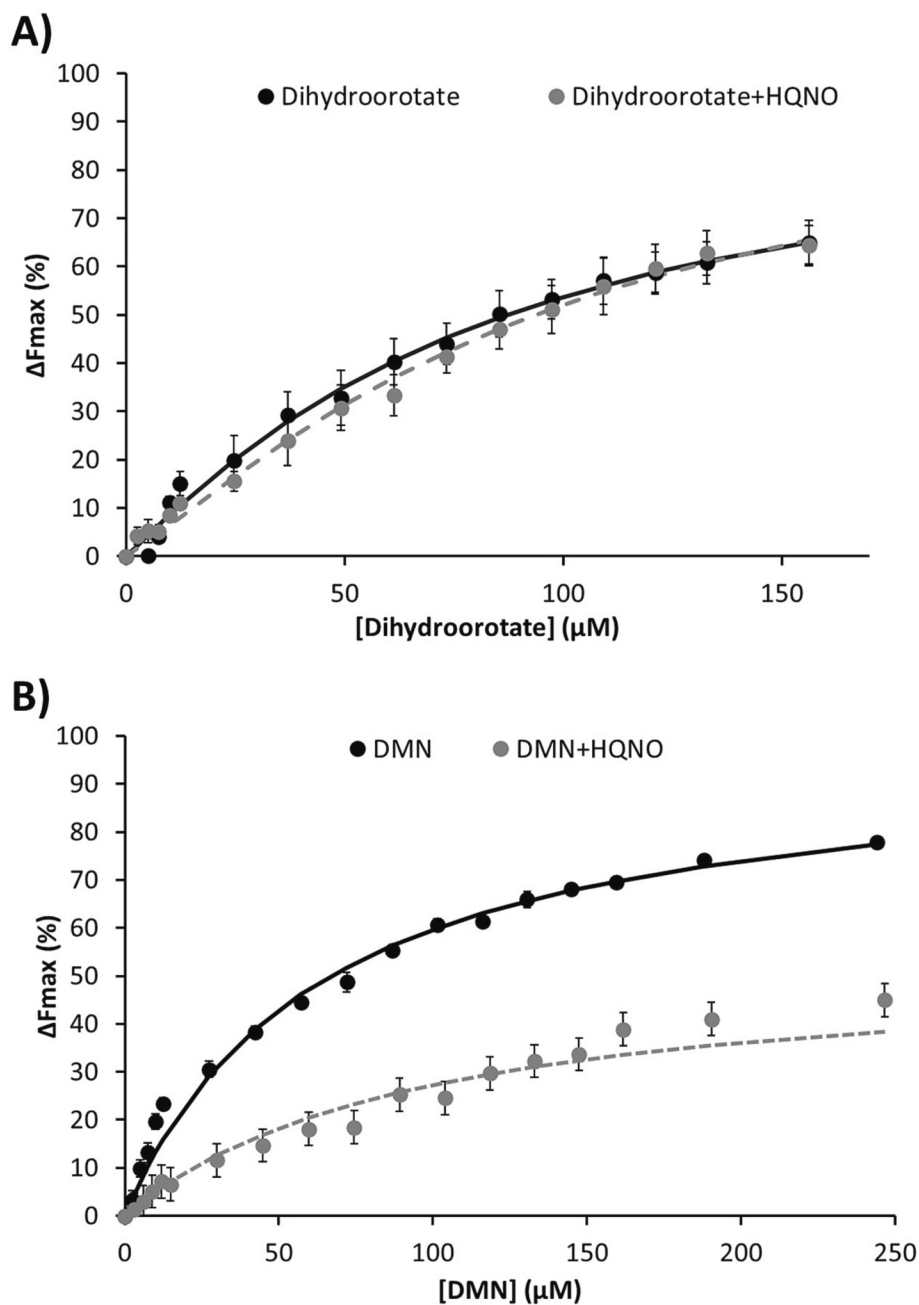
Fig. 4. Protein-substrate interaction studies by fluorescence spectroscopy. DHOQO was excited at 295 nm and the change in the fluorescence emission at 350 nm, ΔF (%), was normalized and represented *versus* the substrate concentration of dihydroorotate (panel A) or DMN (panel B), both in the presence and absence of HQNO (grey dashed lines and black filled lines respectively). Error bars are given in standard deviation. Lines represent the fitted curves using the MWC model equation.

Globally, the lead molecules studied here seem to be less efficient on the bacterial enzyme than on the eukaryotic ones.

To investigate the cellular function of DHOQO from *S. aureus*, we built a knock-out mutant strain of the gene coding for this protein ($\Delta dhoqo$) and analysed its growth fit, general morphology, and metabolic profile in comparison to the wild-type strain (*WT, S. aureus* MW2).

S. aureus growths were performed in TSB medium containing 14 mM glucose, monitoring both the optical density at 600 nm (OD_{600}) and the pH (Fig. 6). The *WT* strain reached a maximum OD_{600} of approximately 7, presenting an exponential growth phase roughly from the 1.5 h to 7 h (Fig. 6, panel A). This exponential phase was also characterized by a significant decrease in the pH growth medium from 7 to <5.5 (Fig. 6, panel B), a value that was kept constant until 9 h of growth. By comparison, $\Delta dhoqo$ showed a considerably altered growth profile, not only

reaching a lower maximum OD_{600} of ~3.5, but also having a different pH profile. Despite the final pH value measured being close to 5.5, the $\Delta dhoqo$ strain reached this value at around 8 h of growth, while the *WT* strain reached the same value at 4 h. This result illustrates the global impact of DHOQO in the metabolism of *S. aureus*.

We also investigated the expression of the *dhoqo* gene using a promotor fusion approach. The promotor fusion strain ("*dhoqo promotor:: GFP*") was built by adding a 700 bp sequence corresponding to the DHOQO coding gene promotor fused to a GFP coding sequence. This strain allowed us to monitor the increase in fluorescence due to the production of that GFP. Since the gene coding for GFP is under the control of the promotor of DHOQO, production of GFP correlates with the expression of the DHOQO coding gene (Fig. S5). We observed an increase in fluorescence starting from ~4 h of growth, reaching
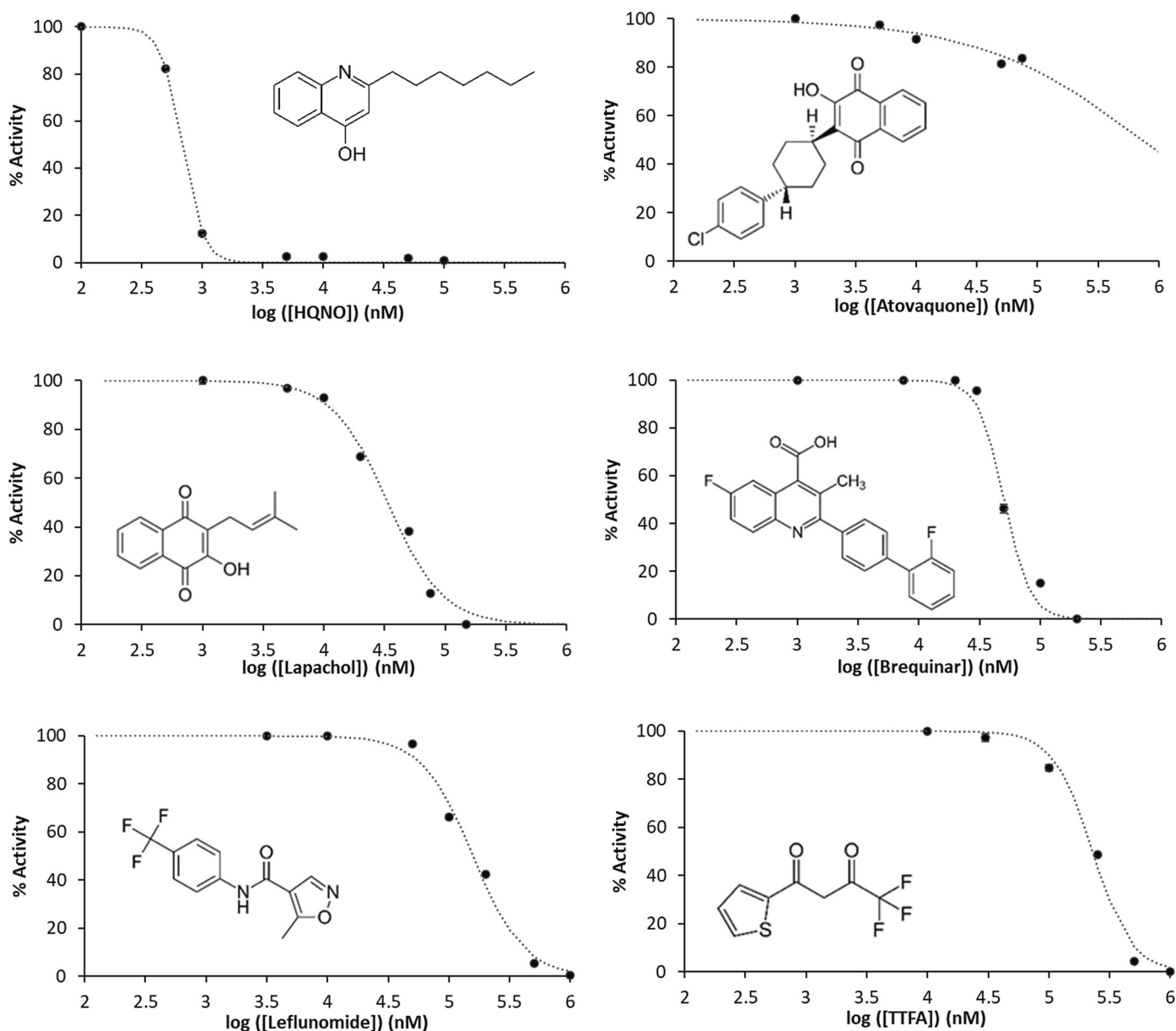
Fig. 5. Inhibitory studies of different classes of inhibitors acting on DHOQO from *S. aureus*. Inhibition effect was studied by plotting the percentage of enzymatic activity (100 % activity being measured in absence of inhibitor) *vs* the logarithm of inhibitor concentration in nM. Inflection points of the obtained curves allowed calculating the respective IC$_{50}$ for HQNO, Atovaquone, Lapachol, Brequinar, Leflunomide and TTFA. All experiment points were measured in triplicates and error bars are presented as the standard deviation of such triplicates. Enzymatic activity quantified quinol formation (μmol/min/mg) by measuring the absorbance variation at 270 nm.

Table 1

Summary of currently determined IC$_{50}$ (given in μM) values for DHOQOs of different organisms for different classes of inhibitors.

	IC$_{50}$ (μM)			
	S. aureus	*H. sapiens*	*P. falciparum*	*R. norvegicus*
HQNO	0.68 ± 0.05	–	–	–
Brequinar	50 ± 9	0.007 [73]	–	0.367 [74]
Atovaquone	740 ± 125	14.5 [75]	1.22 [76]	0.698 [75]
Leflunomide	157 ± 11	98 [74]	–	6.3 [74]
Lapachol	33 ± 8	0.13 [77]	123.5 [76]	–
TTFA	228 ± 9	–	–	–

DHOQO Knock-Out affects cell fitness and morphology.

maximum expression levels at ~6 h. However, no information on DHOQO half-life is known, and as such, the following decrease in fluorescence may not correlate directly to a decrease in the level of the protein. The maximum gene expression/protein production levels observed also correspond to the growth phase at which the most significant OD$_{600}$ differences were observed between *WT* and *Δdhoqo*.

We evaluated the impact of the absence of DHOQO in cell morphology using atomic force microscopy (AFM). Most cells, obtained from growths in solid agar TSB plate, were shown to be organized in clumps of ten or more cells (Fig. S6) but in some cases, cell triads or even individual cells could be observed (Fig. S7, panels A and B). Cells from *WT* and *Δdhoqo* strains present significant differences on their morphology (Fig. S7, panel C). *Δdhoqo* strain cells were consistently larger and had their rugosity altered when comparing with *WT* strain (Fig. S7, panel C). A slower division cycle, combined with larger cells
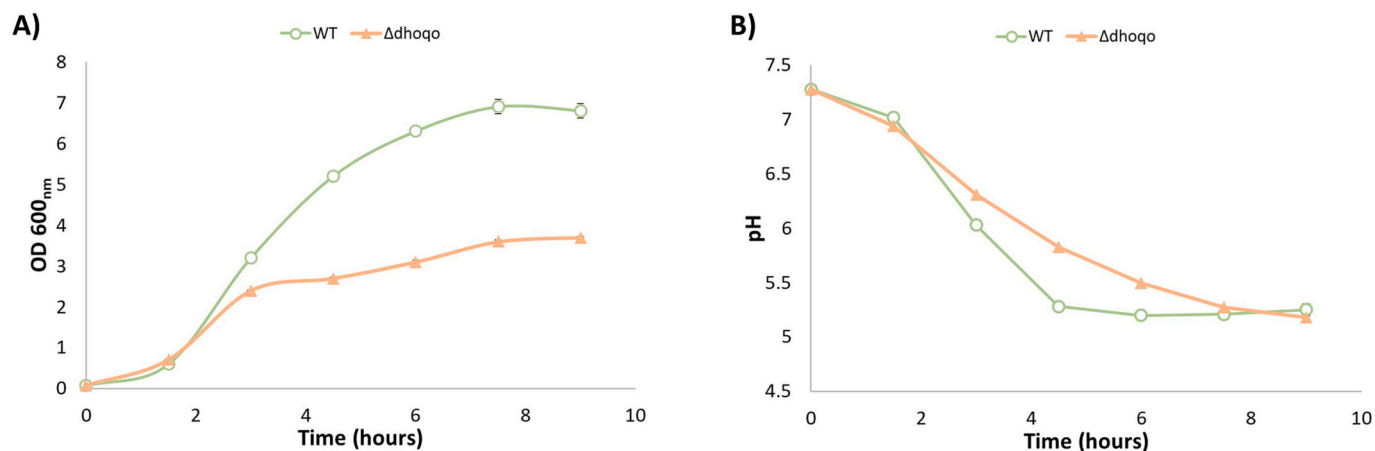
Fig. 6. Cell growth of *S. aureus* MW2 and Δ*dhoqo* strains. Growth was followed by measuring the absorbance at 600 nm (panel A, OD$_{600nm}$) and the corresponding pH value (panel B) every 1.5 h. Each time point was measured in triplicates with error bars given in standard deviation. Green lines correspond to *S. aureus* MW2 (WT) strain and orange lines correspond to Δ*dhoqo* strain.

and an altered surface rugosity, suggests that cells would spend more time in the later phases of division, having trouble proceeding with their division mechanisms [78,79]. This hampering of their growth rates may result from restrictions in energy due to the affected energy metabolism (as DHOQO is part of the respiratory chain) and/or in nucleotides availability caused by the disrupted pyrimidine synthetic pathway (key for structural nucleotide synthesis for DNA and RNA production).

DHOQO mutation affects cell fitness through the pyrimidine synthesis and not the central energy pathway.

In order to explore possible restrictions in energy and/or in nucleotides availability as causes for the observed consequences of *dhoqo* gene deletion, we performed a thorough NMR-based metabolomic analysis. We studied *WT* and Δ*dhoqo* strains grown in TSB medium, and Δ*dhoqo*

strain grown in TSB medium supplemented with 100 μM uracil. Briefly, for each condition, extracellular metabolites were identified through their characteristic peaks profile in ^{1}H NMR spectra (*e.g.*, acetate, ethanol, glucose, lactate, pyruvate, trehalose, and uracil). For each metabolite, one peak was selected and integrated for further quantitative analysis (the list of quantified molecules and their selected NMR peak in ^{1}H chemical shift and multiplicity are shown in Table S4). A complete profile of the concentration change of these metabolites was obtained for each growth during 9 h under aerobic conditions (Fig. S8, S9 and S10). In general, a decrease in extracellular levels means that the molecule is being imported to the cell and likely being consumed. Likewise, an increase in extracellular levels is probably a result of excessive production inside the cells leading to its excretion.
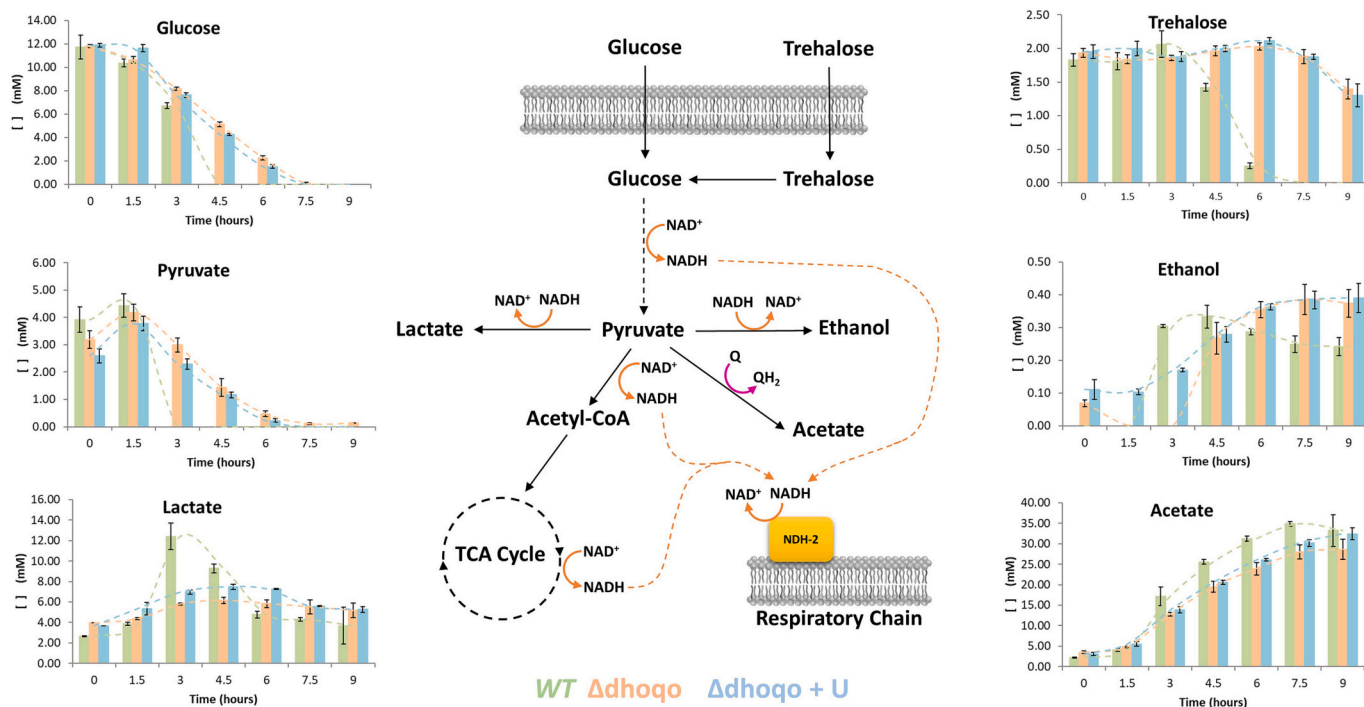

Fig. 7. Energy metabolism of *S. aureus* and profile of the extracellular concentration of the main metabolites involved. Glucose is imported into cells and is metabolized by the glycolytic pathway. The produced pyruvate may follow one (or several) of the represented pathways (black arrows). NADH/NAD$^+$ production (orange arrows) is highlighted for each pathway (dashed lines represent NADH feeding the respiratory chain by the type 2 NADH:quinone oxidoreductase, NDH-2). The side panels represent the extracellular concentration, in mM, of the main metabolites, over a 9 h aerobic growth in TSB medium (green, *WT* strain; orange, Δ*dhoqo* strain; and blue, Δ*dhoqo* strain grown in TSB supplemented with uracil). Metabolites were identified and quantified through ^{1}H NMR spectroscopy.

The initial concentration of glucose (the main carbon source) on the culture media was approximately 12 mM which is readily consumed as cells rely on their glycolytic pathway for the first step of their catabolism. Cells from *WT* strain depleted extracellular glucose levels sometime between 3 and 4.5 h of growth, while those from *Δdhoqo* strain took about 6 to 7.5 h to do the same (Fig. 7). The extinction of glucose from the medium leads cells to start using trehalose (a glucose-based disaccharide) as the main energy source, as well as lowering their growth rate (decrease of exponential growth). Trehalose extracellular levels were kept unchanged ($\approx$ 2 mM) until no glucose was left in the medium (Fig. 7). This was observed both for *WT* and *Δdhoqo* strains. The difference in glucose (followed by trehalose) consumption levels agrees with the lower growth rates previously mentioned for the *Δdhoqo* strain (Fig. 6) and indicates an overall slower growth metabolism when DHOQO is absent.

As glycolysis takes place, glucose is oxidized to pyruvate which can then be further metabolized by different pathways according to the cell's needs. The fact that we do not observe an increase in extracellular pyruvate levels (Fig. 7) indicates that no accumulation is happening inside cells (at least not to a point at which pyruvate is excreted). In fact, the amount of pyruvate present in the growth medium is quickly consumed, pointing that pyruvate is being readily used inside cells. Similarly to what happens with glucose and trehalose, *WT* strain imports extracellular pyruvate faster than *Δdhoqo* strain (1.5 *vs* 6 h), again corroborating the slower growth rates observed for the mutant. In *S. aureus*, pyruvate may be further metabolized in different ways, which involves its reduction to lactate (lactic fermentation) or to ethanol (alcoholic fermentation); its oxidation to formate or to acetyl-CoA (feeding the TCA cycle); its oxidative decarboxylation to acetate; its transamination to alanine; or its two-step decarboxylation into acetoin. Fig. 7 illustrates the main pathways that, according to our data, are active in our experimental conditions. In *WT* strain, concomitantly to glucose/trehalose consumption, extracellular accumulation of lactate and acetate is observed, indicating that these are the main two products of pyruvate metabolism. A slight accumulation of ethanol is also detected, but clearly in smaller amounts ($\approx$ 0.4 mM). In these glucose rich conditions, *S. aureus* is known to adopt a mechanism known as carbon catabolite repressor [80], which leads to the shutdown of the TCA cycle. In this case, pyruvate is not further oxidized through this metabolic cycle and must be directed to alternative pathways.

In the case of *WT* strain, by the 3 h of growth, 6 mM of glucose (and roughly 4 mM of pyruvate) were already fully consumed. By that time, 15 mM and 12 mM of acetate and lactate, respectively, were already accumulated in the medium which is thought to cause the measured decrease in the pH of the medium (from 7.2 to 6, Fig. 6 panel B). Up to this point it seems that pyruvate metabolism is divided between its oxidative decarboxylation to acetate and reduction to lactate. In the first case, the organism is respiring, as NADH (produced in the oxidation of glucose to pyruvate) and quinol (produced by the oxidative decarboxylation of pyruvate to acetate), are oxidized by the respiratory chain. In the second case, the organism is fermenting, as oxidation of NADH occurs by the reduction of pyruvate to lactate. During this early growth stage (lag phase and early exponential phase) part of the pyruvate is also directed to acetoin formation (Fig. S8), which does not have a direct impact on the NADH/NAD$^+$ ratio.

From this point onwards, as glucose is no longer available, there is a shift in the energy metabolism. Acetate keeps accumulating, reaching ~35 mM by 7.5 h of growth and lactate starts being consumed from the growth medium (returning to concentrations close to the initial ones). This equilibrium between acetate production and lactate consumption justifies the observation that pH values around 6 are kept until the end of the growth. This shift in the central energy metabolism, when glucose is no longer available (hence the rate of NAD$^+$ to NADH conversion is decreased), leads to an inversion in the pyruvate to lactate conversion, being now lactate the main carbon and energy source. In this phase of the growth (4.5 h onwards) acetoin and ethanol production stabilize

with extracellular concentrations of 3 mM and 300 μM respectively. At 9 h of growth the WT strain starts to consume acetate, in fact, *S. aureus* MW2 is known to be able to use acetate as the main carbon source [81]. In this case the carbon catabolite repressor mechanism is no longer active and the TCA cycle takes place.

When we performed a similar analysis for the *Δdhoqo* strain we noticed that the differences observed corroborate the significantly slower growth rate (both in the media with and without uracil). In general, the profile of the changes in concentration of the identified metabolites seems to follow the same behaviour as that observed for the *WT* strain but with a time delay (as already mentioned for glucose, trehalose, and pyruvate). Pyruvate seems to be metabolized by the same two main pathways in the *Δdhoqo* strain as in the *WT* strain. As glucose, trehalose and pyruvate extracellular levels decrease (with extracellular pyruvate levels being depleted around 6 h of growth), ethanol, lactate and acetate levels increase. As for the *WT* strain, in the case of the *Δdhoqo* strain acetate and lactate concentrations increase justifies the observed decrease in extracellular medium pH. Since neither acetate nor lactate reach concentrations as high as those observed for the *WT* strain (with maxima at 27 and 6 mM for acetate and lactate respectively), the decrease in pH levels is also not so pronounced. More generally, it seems the *Δdhoqo* strain, similarly to *WT,* suffered a shift from one phase of the growth to another, adapting its metabolism according to the available carbon and/or energy resources. The main difference lies in the fact that no lactate concentration spike is observed. This behaviour seems to indicate that the *Δdhoqo* strain does not need to redirect so much pyruvate to the lactic fermentation pathway, probably as it is able to manage the lower NADH/NAD$^+$ ratio resulting from a decreased glucose conversion ratio (which is a direct consequence of the lower growth rates). Our hypothesis is based on the fact that NAD$^+$ is converted to NADH in the glycolytic pathway and that the fermenting pathway is a direct answer to the increase in the NADH/NAD$^+$ ratio [82]. In the *Δdhoqo* strain, the influx is considerably lower, so the need to use a fermenting pathway is also lower.

Together these observations seem to indicate that no fundamental difference is observed in the energy metabolism of the *Δdhoqo* strain, comparing to that of the *WT* strain. The measured differences in lactate uptake are a consequence of the impaired growth rate and not the cause of it. In this case the explanation for the observed impact of the DHOQO mutation is likely related to the other metabolic pathway in which the enzyme is directly involved: the pyrimidine biosynthetic pathway.

Pyrimidine biosynthesis may be performed either through the designated *de novo* or the *salvage* pathways. In the *de novo* pathway, a sequence of six reactions transform glutamine in uridine monophosphate (UMP), a necessary precursor for DNA and RNA synthesis. The salvage pathway bypasses the *de novo* pathway as external uracil or uridine may be directly used to feed the UMP pool. Fig. 8 illustrates the two pathways and the enzymes (numbered "1" to "11") assigned for *S. aureus*. As for other pathways, cells may adapt and use either the *salvage* or the *de novo* pathway. For example, the inhibition of the *de novo* pyrimidine pathway in *Solanum tuberosum* leads to an increase in the salvage pathway utilization [83]. An even more extreme example is the case of *Trypanosoma brucei*, in which the *de novo* pathway is completely absent, but the presence of the salvage pathway fully compensates for it [84]. For most other organisms, including *S. aureus*, the relative contribution of each pathway is not known.

As the precursor of nucleotide synthesis, UMP is a key metabolite to sustain cellular division, and as such the need for UMP increases with the rate of cell growth. In the *WT* strain, UMP synthesis may occur through both pathways, as DHOQO (enzyme "4" in Fig. 8) is still encoded in the genome and uracil is present in the medium. Contrarily, the *Δdhoqo* strain is expected to use exclusively the salvage pathway in order to compensate for the lack of the gene coding for DHOQO. One direct metabolic marker of the usage of the salvage pathway is the decrease of the concentration of uracil in the growth medium. Fig. 8 also shows the profile of the change on the extracellular concentration of
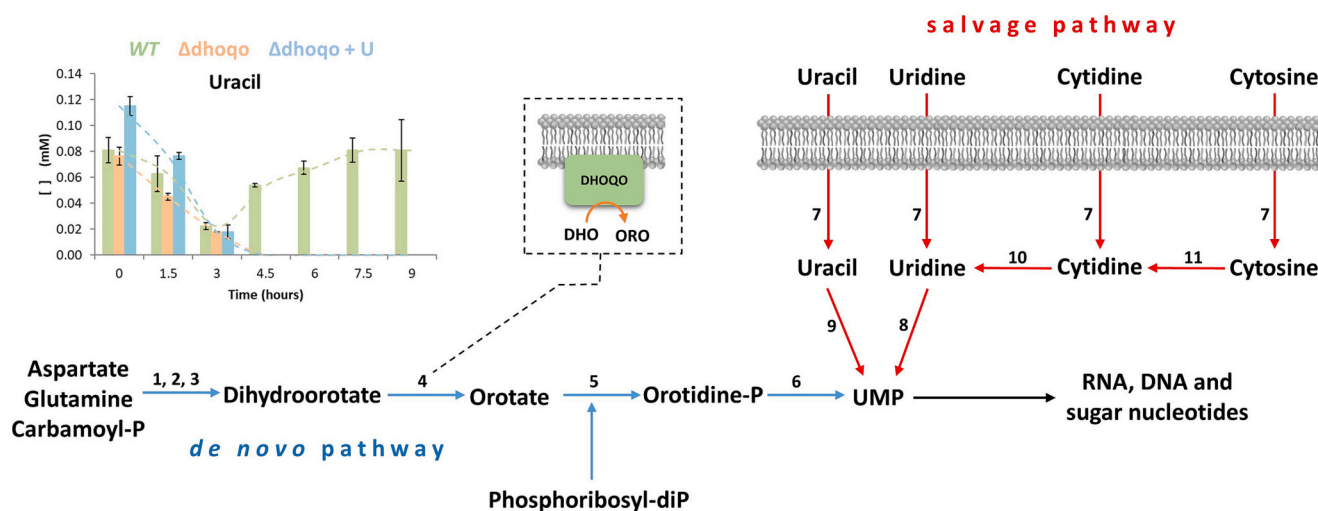
Fig. 8. *S. aureus'* pyrimidine biosynthesis pathways and uracil extracellular concentration profile. The two pyrimidine biosynthesis pathways are represented: salvage pathway (in red arrows) and *de novo* pathway (in blue arrows). The numbers correspond to the enzymes catalysing each reaction: "1" – carbamoyl-phosphate synthase (Uniprot ID P63730 + P58940); "2" – aspartate transcarbamoylase (Uniprot ID P65619); "3" – dihydroorotatase (Uniprot ID P65907); "4" – dihydroorotate:quinone oxidoreductase (Uniprot ID A0A0H3K1V6); "5" – orotate phosphoribosyl transferase (Uniprot ID Q8NX25); "6" – orotidine-5-phosphate decarboxylase (Uniprot ID P65596); "7" – uracil permease (Uniprot ID A0A0H3JZU1); "8" – uridine kinase (Uniprot ID P67412); "9" – uracil phosphoribosyl transferase (Uniprot ID P65945 + P67397); "10" – cytidine deaminase (Uniprot ID A0A0H3JXQ8); "11" – pyrimidine-nucleoside phosphorylase (Uniprot ID Q8NVF6). The side panel represents the uracil extracellular concentration, in mM, over a 9-h aerobic growth in TSB medium (green, *WT* strain; orange, *Δdhoqo* strain; and blue, *Δdhoqo* strain grown in TSB supplemented with uracil). Uracil was identified and quantified through ^{1}H NMR spectroscopy. DHOQO reaction scheme is illustrated in the dashed box with "DHO" and "ORO" corresponding to the electron donor and acceptor, dihydroorotate and orotate respectively.

uracil during the same growth period discussed above for the energy metabolism. It is possible to observe that both for *WT* (green bars) and for *Δdhoqo* (orange bars) strains, uracil is readily consumed from the medium. Uracil concentration profile is similar for the two strains and reaches its minimum around the 3 h of growth. From Fig. 6 we can observe that it is from this point onwards that the growths (the measured OD_{600}) of both strains starts to differentiate, with *WT* strain continuing to increase and *Δdhoqo* strain stagnating. This similar behaviour seems to indicate that both strains utilize the salvage pathway in the early hours of growth. As the medium became depleted of uracil (around the 3 h), the *Δdhoqo* strain is not able to utilize the salvage pathway any longer and its growth stops, while the *WT* strain may switch to the *de novo* pathway. The hypothesis that uracil is sustaining the salvage pathway that is being used is further supported by the growth profile of the *Δdhoqo* strain grown in uracil supplemented TSB (blue line in Fig. S11). The growth of the *Δdhoqo* strain in this condition not only reaches a higher final OD_{600} comparing to that of the *Δdhoqo* strain without uracil, but even comparing to the *WT* strain it seems to be able to grow faster in the early stages of growth (Fig. S11) due to a higher concentration of uracil in the medium (blue bars in Fig. 8), roughly 100 μM. Even so, after the 3 h, extracellular uracil is depleted and the *Δdhoqo* strain is still not able to switch to the *de novo* pathway as so its growth is severely slowed. The *Δdhoqo* strain is still able to slowly grow after the 3 h probably due to utilization of a different metabolite fuelling the salvage pathway, which is either less efficient or is present in smaller amounts in the medium. Two possibilities, in this case, are cytidine and cytosine (later converted to uridine), which we could not identify through our approach.

In the case of the *WT* strain, from the 3 h onwards (and concomitantly with the switch from a mixed fermentative metabolism to a purely respiratory one), this strain seems to use the *de novo* pyrimidine biosynthesis pathway. In fact, this is corroborated by the fluorescence profile measured for the *dhoqo promotor::GFP* strain, which indicates that the protein starts to be significantly produced after 4 h of growth (Fig. S5). At that point, an inversion in the uracil concentration profile occurs, as it starts increasing up to the initial concentrations around the 9 h of growth. This result is unexpected but does not contradict the

previous hypothesis. We can speculate that as the *de novo* pathway starts to be activated, the UMP pool builds up, unbalancing the pathway towards the production of uracil (Fig. 8 reactions "7", "8" and "9"). The reversibility of the reactions involved has been previously shown to occur in plants [85].

4. Conclusions

In this work, we unveil the DHOQO from *S. aureus*. We report the first successful isolation and characterization of this enzyme, the first from a Gram-positive organism.

We performed a thorough molecular characterization, showing unequivocally its quinone reductase activity. By identifying the presence of a quinone binding motif on its N-terminal and by showing, through fluorescence titration experiments, that the two substrates bind at different locations in the protein, we corroborate the currently accepted binding location for the quinone at the *si*-side of the flavin, in the N-terminal domain. This FMN containing monotopic enzyme interacted preferentially with a menaquinone analogue, presented a Michaelis-Menten behaviour for both substrates and was inhibited by different classes of molecules. We showed for the first time that DHOQOs are inhibited by HQNO, a known anti-staphylococcal agent produced by a competing bacterium, *P. aeruginosa*, during host colonization. Our exploratory inhibition study was expanded to some of classic DHOQO inhibitors as Lapachol, Brequinar, Leflunomide and Atovaquone; and to some previously untested molecules like TTFA.

We also investigated the cellular function of this enzyme by deleting the DHOQO coding gene from *S. aureus* MW2 (*Δdhoqo*). Gene deletion led to a viable knock-out strain with relevant morphological and metabolic differences in relation to the *WT*. *Δdhoqo* strain showed lower growth rates when comparing to the *WT* strain, which we speculate to lead to the observed increase in the cellular volume.

Despite the observed differences in the glucose consumption and lactate accumulation levels, we conclude that the main impact of the DHOQO coding gene deletion is on the pyrimidine biosynthesis.

Declaration of competing interest

The authors declare that they have no known competing financial interests or personal relationships that could have appeared to influence the work reported in this paper.

Data availability

Data will be made available on request.

Acknowledgments

Appendix A. Supplementary data

Supplementary data to this article can be found online at https://doi.org/10.1016/j.bbabio.2022.148948.

References

[1] S.Y.C. Tong, J.S. Davis, E. Eichenberger, T.L. Holland, V.G. Fowler, *Staphylococcus aureus* infections: epidemiology, pathophysiology, clinical manifestations, and management, Clin. Microbiol. Rev. 28 (2015) 603–661, https://doi.org/10.1128/CMR.00134-14.

[2] H.F. Chambers, F.R. DeLeo, Waves of resistance: *Staphylococcus aureus* in the antibiotic era, Nat. Rev. Microbiol. 7 (2009) 629–641, https://doi.org/10.1038/nrmicro2200.

[3] R.M. Klevens, Invasive methicillin-resistant *Staphylococcus aureus* infections in the United States, JAMA 298 (2007) 1763, https://doi.org/10.1001/jama.298.15.1763.

[4] S. Fuchs, J. Pané-Farré, C. Kohler, M. Hecker, S. Engelmann, Anaerobic gene expression in *Staphylococcus aureus*, J. Bacteriol. 189 (2007) 4275–4289, https://doi.org/10.1128/JB.00081-07.

[5] K.A. Burke, J. Lascelles, Nitrate reductase system in *Staphylococcus aureus* wild type and mutants, J. Bacteriol. 123 (1975) 308–316, https://doi.org/10.1128/JB.123.1.308-316.1975.

[6] F. Götz, S. Mayer, Both terminal oxidases contribute to fitness and virulence during organ-specific *Staphylococcus aureus* colonization, MBio 4 (2013), e00976-13, https://doi.org/10.1128/mBio.00976-13.

[7] B.C. Marreiros, F. Calisto, P.J. Castro, A.M. Duarte, F.V. Sena, A.F. Silva, F. M. Sousa, M. Teixeira, P.N. Refojo, M.M. Pereira, Exploring membrane respiratory chains, Biochim. Biophys. Acta Bioenerg. 2016 (1857) 1039–1067, https://doi.org/10.1016/j.bbabio.2016.03.028.

[8] P.N. Refojo, F.V. Sena, F. Calisto, F.M. Sousa, M.M. Pereira, The plethora of membrane respiratory chains in the phyla of Life, in: Adv. Microb. Physiol, Academic Press, 2019, pp. 331–414, https://doi.org/10.1016/bs.ampbs.2019.03.002.

[9] L.A. Schurig-Briccio, T. Yano, H. Rubin, R.B. Gennis, Characterization of the type 2 NADH:menaquinone oxidoreductases from *Staphylococcus aureus* and the bactericidal action of phenothiazines, Biochim. Biophys. Acta Bioenerg. 2014 (1837) 954–963, https://doi.org/10.1016/j.bbabio.2014.03.017.

[10] F.V. Sena, F.M. Sousa, A.S.F. Oliveira, C.M. Soares, T. Catarino, M.M. Pereira, Regulation of the mechanism of type-II NADH: quinone oxidoreductase from *S. aureus*, Redox Biol. 16 (2018) 209–214, https://doi.org/10.1016/j.redox.2018.02.004.

[11] X. Zhang, K.W. Bayles, S. Luca, *Staphylococcus aureus* CidC is a pyruvate: menaquinone oxidoreductase, Biochemistry 56 (2017) 4819–4829, https://doi.org/10.1021/acs.biochem.7b00570.

[12] J. Shen, H. Peng, Y. Zhang, J.C. Trinidad, D.P. Giedroc, *Staphylococcus aureus* sqr encodes a type II sulfide: quinone oxidoreductase and impacts reactive sulfur speciation in cells, Biochemistry 55 (2016) 6524–6534, https://doi.org/10.1021/acs.biochem.6b00714.

[13] R.A.G. Reis, F.A. Calil, P.R. Feliciano, M.P. Pinheiro, M.C. Nonato, The dihydroorotate dehydrogenases: past and present, Arch. Biochem. Biophys. 632 (2017) 175–191, https://doi.org/10.1016/j.abb.2017.06.019.

[14] J. Leban, D. Vitt, Human dihydroorotate dehydrogenase inhibitors, a novel approach for the treatment of autoimmune and inflammatory diseases, Arzneimittelforschung 61 (2011) 66–72, https://doi.org/10.1055/s-0031-1296169.

[15] R.I. Christopherson, S.D. Lyons, P.K. Wilson, Inhibitors of de novo nucleotide biosynthesis as drugs, Acc. Chem. Res. 35 (2002) 961–971, https://doi.org/10.1021/ar0000509.

[16] M.C. Nonato, R.A.P. de Pádua, J.S. David, R.A.G. Reis, G.P. Tomaleri, H. D'Muniz Pereira, F.A. Calil, Structural basis for the design of selective inhibitors for *Schistosoma mansoni* dihydroorotate dehydrogenase, Biochimie 158 (2019) 180–190, https://doi.org/10.1016/j.biochi.2019.01.006.

[17] M. Loffler, L. Fairbanks, E. Zameitat, A. Marinaki, H. Simmonds, Pyrimidine pathways in health and disease, Trends Mol. Med. 11 (2005) 430–437, https://doi.org/10.1016/j.molmed.2005.07.003.

[18] F.A. Calil, J.S. David, E.R.C. Chiappetta, F. Fumagalli, R.B. Mello, F.H.A. Leite, M. S. Castilho, F.S. Emery, M.C. Nonato, Ligand-based design, synthesis and biochemical evaluation of potent and selective inhibitors of *Schistosoma mansoni* dihydroorotate dehydrogenase, Eur. J. Med. Chem. 167 (2019) 357–366, https://doi.org/10.1016/j.ejmech.2019.02.018.

[19] D. Boschi, A.C. Pippione, S. Sainas, M.L. Lolli, Dihydroorotate dehydrogenase inhibitors in anti-infective drug research, Eur. J. Med. Chem. 183 (2019), 111681, https://doi.org/10.1016/j.ejmech.2019.111681.

[20] W.H. Taylor, G.D. Novelli, Enzymes of the pyrimidine pathway in *Escherichia coli* I, J. Bacteriol. 88 (1964) 99–104, https://doi.org/10.1128/JB.88.1.99-104.1964.

[21] M.F. Garavito, H.Y. Narvaez-Ortiz, D.C. Pulido, M. Löffler, H.S. Judelson, S. Restrepo, B.H. Zimmermann, Phytophthora infestans dihydroorotate dehydrogenase is a potential target for chemical control – a comparison with the enzyme from *Solanum tuberosum*, Front. Microbiol. 10 (2019), https://doi.org/10.3389/fmicb.2019.01479.

[22] A. Ullrich, W. Knecht, J. Piskur, M. Löffler, Plant dihydroorotate dehydrogenase differs significantly in substrate specificity and inhibition from the animal enzymes, FEBS Lett. 529 (2002) 346–350, https://doi.org/10.1016/S0014-5793(02)03425-7.

[23] M. Löffler, W. Knecht, J. Rawls, A. Ullrich, C. Dietz, *Drosophila melanogaster* dihydroorotate dehydrogenase: the N-terminus is important for biological function in vivo but not for catalytic properties in vitro, Insect Biochem. Mol. Biol. 32 (2002) 1159–1169, https://doi.org/10.1016/S0965-1748(02)00052-8.

[24] M.A. Hortua Triana, D. Cajiao Herrera, B.H. Zimmermann, B.A. Fox, D.J. Bzik, Pyrimidine pathway-dependent and -independent functions of the *Toxoplasma gondii* mitochondrial dihydroorotate dehydrogenase, Infect. Immun. 84 (2016) 2974–2981, https://doi.org/10.1128/IAI.00187-16.

[25] M. Hansen, Inhibitor binding in a class 2 dihydroorotate dehydrogenase causes variations in the membrane-associated N-terminal domain, Protein Sci. 13 (2004) 1031–1042, https://doi.org/10.1110/ps.03533004.

[26] R.M. Mori, M.A.A. Aleixo, L.C.C. Zapata, F.A. Calil, F.S. Emery, M.C. Nonato, Structural basis for the function and inhibition of dihydroorotate dehydrogenase from *Schistosoma mansoni*, FEBS J. (2020), febs.15367, https://doi.org/10.1111/febs.15367.

[27] M. Davies, T. Heikkilä, G.A. McConkey, C.W.G. Fishwick, M.R. Parsons, A. P. Johnson, Structure-based design, synthesis, and characterization of inhibitors of human and *Plasmodium falciparum* dihydroorotate dehydrogenases †, J. Med. Chem. 52 (2009) 2683–2693, https://doi.org/10.1021/jm800963t.

[28] E. Zameitat, Z. Gojkovic, W. Knecht, J. Piskur, M. Löffler, Biochemical characterization of recombinant dihydroorotate dehydrogenase from the opportunistic pathogenic yeast *Candida albicans*, FEBS J. 273 (2006) 3183–3191, https://doi.org/10.1111/j.1742-4658.2006.05327.x.

[29] E. Zameitat, W. Knecht, J. Piškur, M. Löffler, Two different dihydroorotate dehydrogenases from yeast *Saccharomyces kluyveri*, FEBS Lett. 568 (2004) 129–134, https://doi.org/10.1016/j.febslet.2004.05.017.

[30] R.L. Fagan, B.A. Palfey, Roles in binding and chemistry for conserved active site residues in the class 2 dihydroorotate dehydrogenase from *Escherichia coli*, Biochemistry 48 (2009) 7169–7178, https://doi.org/10.1021/bi900370s.

[31] R.A. Copeland, J. Marcinkeviciene, T.S. Haque, L.M. Kopcho, W. Jiang, K. Wang, L. D. Ecret, C. Sizemore, K.A. Amsler, L. Foster, S. Tadesse, A.P. Combs, A.M. Stern, G. L. Trainor, A. Slee, M.J. Rogers, F. Hobbs, *Helicobacter pylori*-selective antibacterials based on inhibition of pyrimidine biosynthesis, J. Biol. Chem. 275 (2000) 33373–33378, https://doi.org/10.1074/jbc.M004451200.

[32] S. Liu, E.A. Neidhardt, T.H. Grossman, T. Ocain, J. Clardy, Structures of human dihydroorotate dehydrogenase in complex with antiproliferative agents, Structure 8 (2000) 25–33, https://doi.org/10.1016/S0969-2126(00)00077-0.

[33] P.T.P. Bedingfield, D. Cowen, P. Acklam, F. Cunningham, M.R. Parsons, G. A. McConkey, C.W.G. Fishwick, A.P. Johnson, Factors influencing the specificity of inhibitor binding to the human and malaria parasite dihydroorotate dehydrogenases, J. Med. Chem. 55 (2012) 5841–5850, https://doi.org/10.1021/jm300157n.

[34] M. Erra, I. Moreno, J. Sanahuja, M. Andrés, R.F. Reinoso, E. Lozoya, P. Pizcueta, N. Godessart, J.C. Castro-Palomino, Biaryl analogues of teriflunomide as potent DHODH inhibitors, Bioorg. Med. Chem. Lett. 21 (2011) 7268–7272, https://doi.org/10.1016/j.bmcl.2011.10.052.

[35] I. Fritzson, B. Svensson, S. Al-Karadaghi, B. Walse, U. Wellmar, U.J. Nilsson, D. da Graça Thrige, S. Jönsson, Inhibition of human DHODH by 4-hydroxycoumarins, fenamic acids, and N -(alkylcarbonyl)anthranilic acids identified by structure-guided fragment selection, ChemMedChem 5 (2010) 608–617, https://doi.org/10.1002/cmdc.200900454.

[36] L.R. McLean, Y. Zhang, W. Degnen, J. Peppard, D. Cabel, C. Zou, J.T. Tsay, A. Subramaniam, R.J. Vaz, Y. Li, Discovery of novel inhibitors for DHODH via virtual screening and X-ray crystallographic structures, Bioorg. Med. Chem. Lett. 20 (2010) 1981–1984, https://doi.org/10.1016/j.bmcl.2010.01.115.

[37] B. Walse, V.T. Dufe, B. Svensson, I. Fritzson, L. Dahlberg, A. Khairoullina, U. Wellmar, S. Al-Karadaghi, The structures of human dihydroorotate dehydrogenase with and without inhibitor reveal conformational flexibility in the inhibitor and substrate binding sites †, Biochemistry 47 (2008) 8929–8936, https://doi.org/10.1021/bi8003318.

[38] R. Baumgartner, M. Walloschek, M. Kralik, A. Gotschlich, S. Tasler, J. Mies, J. Leban, Dual binding mode of a novel series of DHODH inhibitors, J. Med. Chem. 49 (2006) 1239–1247, https://doi.org/10.1021/jm0506975.

[39] D.E. Hurt, J. Widom, J. Clardy, Structure of plasmodium falciparum dihydroorotate dehydrogenase with a bound inhibitor, Acta Crystallogr. Sect. D Biol. Crystallogr. 62 (2006) 312–323, https://doi.org/10.1107/S0907444905042642.

[40] X. Deng, R. Gujjar, F. El Mazouni, W. Kaminsky, N.A. Malmquist, E.J. Goldsmith, P. K. Rathod, M.A. Phillips, Structural plasticity of malaria dihydroorotate dehydrogenase allows selective binding of diverse chemical scaffolds, J. Biol. Chem. 284 (2009) 26999–27009, https://doi.org/10.1074/jbc.M109.028589.

[41] X. Deng, D. Matthews, P.K. Rathod, M.A. Phillips, The X-ray structure of Plasmodium falciparum dihydroorotate dehydrogenase bound to a potent and selective N -phenylbenzamide inhibitor reveals novel binding-site interactions, Acta Crystallogr. Sect. F: Struct. Biol. Cryst. Commun. 71 (2015) 553–559, https://doi.org/10.1107/S2053230X15000989.

[42] J.M. Coteron, M. Marco, J. Esquivias, X. Deng, K.L. White, J. White, M. Koltun, F. El Mazouni, S. Kokkonda, K. Katneni, R. Bhamidipati, D.M. Shackleford, I. Angulo-Barturen, S.B. Ferrer, M.B. Jiménez-Díaz, F.-J. Gamo, E.J. Goldsmith, W. N. Charman, I. Bathurst, D. Floyd, D. Matthews, J.N. Burrows, P.K. Rathod, S. A. Charman, M.A. Phillips, Structure-guided lead optimization of triazolopyrimidine-ring substituents identifies potent Plasmodium falciparum dihydroorotate dehydrogenase inhibitors with clinical candidate potential, J. Med. Chem. 54 (2011) 5540–5561, https://doi.org/10.1021/jm200592f.

[43] S. Nørager, K.F. Jensen, O. Björnberg, S. Larsen, E. coli dihydroorotate dehydrogenase reveals structural and functional distinctions between different classes of dihydroorotate dehydrogenases, Structure 10 (2002) 1211–1223, https://doi.org/10.1016/S0969-2126(02)00831-6.

[44] F.M. Sousa, P.N. Refojo, M.M. Pereira, Investigating the amino acid sequences of membrane bound dihydroorotate:quinone oxidoreductases (DHOQOs): structural and functional implications, Biochim. Biophys. ActaBioenerg. 1862 (2021), 148321, https://doi.org/10.1016/j.bbabio.2020.148321.

[45] A. Sali, Comparative protein modeling by satisfaction of spatial restraints, Mol. Med. Today 1 (1995) 270–277, https://doi.org/10.1016/S1357-4310(95)91170-7.

[46] X. Deng, S. Kokkonda, F. El Mazouni, J. White, J.N. Burrows, W. Kaminsky, S. A. Charman, D. Matthews, P.K. Rathod, M.A. Phillips, Fluorine modulates species selectivity in the triazolopyrimidine class of Plasmodium falciparum dihydroorotate dehydrogenase inhibitors, J. Med. Chem. 57 (2014) 5381–5394, https://doi.org/10.1021/jm500481t.

[47] J.M. Coteron, M. Marco, J. Esquivias, X. Deng, K.L. White, J. White, M. Koltun, F. El Mazouni, S. Kokkonda, K. Katneni, R. Bhamidipati, D.M. Shackleford, I. Angulo-Barturen, S.B. Ferrer, M.B. Jiménez-Díaz, F.-J. Gamo, E.J. Goldsmith, W. N. Charman, I. Bathurst, D. Floyd, D. Matthews, J.N. Burrows, P.K. Rathod, S. A. Charman, M.A. Phillips, Structure-guided lead optimization of triazolopyrimidine-ring substituents identifies potent Plasmodium falciparum dihydroorotate dehydrogenase inhibitors with clinical candidate potential, J. Med. Chem. 54 (2011) 5540–5561, https://doi.org/10.1021/jm200592f.

[48] R.A. Laskowski, M.W. MacArthur, D.S. Moss, J.M. Thornton, PROCHECK: a program to check the stereochemical quality of protein structures, J. Appl. Crystallogr. 26 (1993) 283–291, https://doi.org/10.1107/S0021889892009944.

[49] R. Weißgerber, Über das 2.3-Dimethyl-naphthalin im Steinkohlenteer, in: Berichte Der Dtsch. Chem. Gesellschaft, A B Ser. 52, 1919, pp. 370–371, https://doi.org/10.1002/cber.19190520227.

[50] M. Arnaud, A. Chastanet, M. Débarbouillé, New vector for efficient allelic replacement in naturally nontransformable, low-GC-content, gram-positive bacteria, Appl. Environ. Microbiol. 70 (2004) 6887–6891, https://doi.org/10.1128/AEM.70.11.6887-6891.2004.

[51] D.R. Nair, J.M. Monteiro, G. Memmi, J. Thanassi, M. Pucci, J. Schwartzman, M. G. Pinho, A.L. Cheung, Characterization of a novel small molecule that potentiates β-lactam activity against gram-positive and gram-negative pathogens, Antimicrob. Agents Chemother. 59 (2015) 1876–1885, https://doi.org/10.1128/AAC.04164-14.

[52] M.G. Pinho, H. de Lencastre, A. Tomasz, Cloning, characterization, and inactivation of the gene pbpC, encoding penicillin-binding protein 3 of Staphylococcus aureus, J. Bacteriol. 182 (2000) 1074–1079, https://doi.org/10.1128/JB.182.4.1074-1079.2000.

[53] R.L. Fagan, M.N. Nelson, P.M. Pagano, B.A. Palfey, Mechanism of flavin reduction in class 2 dihydroorotate dehydrogenases, Biochemistry 45 (2006) 14926–14932, https://doi.org/10.1021/bi060919g.

[54] M.D. Collins, D. Jones, Distribution of isoprenoid quinone structural types in bacteria and their taxonomic implication, Microbiol. Rev. 45 (1981) 316–354, https://doi.org/10.1128/MMBR.45.2.316-354.1981.

[55] F.V. Sena, A.P. Batista, T. Catarino, J.A. Brito, M. Archer, M. Viertler, T. Madl, E. J. Cabrita, M.M. Pereira, Type-II NADH:quinone oxidoreductase from Staphylococcus aureus has two distinct binding sites and is rate limited by quinone reduction, Mol. Microbiol. 98 (2015) 272–288, https://doi.org/10.1111/mmi.13120.

[56] R. Bentley, R. Meganathan, Biosynthesis of vitamin K (menaquinone) in bacteria, Microbiol. Rev. 46 (1982) 241–280, https://doi.org/10.1128/MMBR.46.3.241-280.1982.

[57] M. Hansen, Inhibitor binding in a class 2 dihydroorotate dehydrogenase causes variations in the membrane-associated N-terminal domain, Protein Sci. 13 (2004) 1031–1042, https://doi.org/10.1110/ps.03533004.

[58] J.I. Yeh, U. Chinte, S. Du, Structure of glycerol-3-phosphate dehydrogenase, an essential monotopic membrane enzyme involved in respiration and metabolism, Proc. Natl. Acad. Sci. 105 (2008) 3280–3285, https://doi.org/10.1073/pnas.0712331105.

[59] J. Zhang, F.E. Frerman, J.-J.P. Kim, Structure of electron transfer flavoprotein-ubiquinone oxidoreductase and electron transfer to the mitochondrial ubiquinone pool, Proc. Natl. Acad. Sci. 103 (2006) 16212–16217, https://doi.org/10.1073/pnas.0604567103.

[60] Y. Feng, W. Li, J. Li, J. Wang, J. Ge, D. Xu, Y. Liu, K. Wu, Q. Zeng, J.W. Wu, C. Tian, B. Zhou, M. Yang, Structural insight into the type-II mitochondrial NADH dehydrogenases, Nature 491 (2012) 478–482, https://doi.org/10.1038/nature11541.

[61] J. Petri, Y. Shimaki, W. Jiao, H.R. Bridges, E.R. Russell, E.J. Parker, D. Aragão, G. M. Cook, Y. Nakatani, Structure of the NDH-2 – HQNO inhibited complex provides molecular insight into quinone-binding site inhibitors, Biochim. Biophys. ActaBioenerg. 2018 (1859) 482–490, https://doi.org/10.1016/j.bbabio.2018.03.014.

[62] A.P. Magalhães, P. Jorge, M.O. Pereira, Pseudomonas aeruginosa and Staphylococcus aureus communication in biofilm infections: insights through network and database construction, Crit. Rev. Microbiol. 45 (2019) 712–728, https://doi.org/10.1080/1040841X.2019.1700209.

[63] P. Williams, M. Cámara, Quorum sensing and environmental adaptation in Pseudomonas aeruginosa: a tale of regulatory networks and multifunctional signal molecules, Curr. Opin. Microbiol. 12 (2009) 182–191, https://doi.org/10.1016/j.mib.2009.01.005.

[64] D. Boschi, A.C. Pippione, S. Sainas, M.L. Lolli, Dihydroorotate dehydrogenase inhibitors in anti-infective drug research, Eur. J. Med. Chem. 183 (2019), 111681, https://doi.org/10.1016/j.ejmech.2019.111681.

[65] F.C. Breedveld, Leflunomide: mode of action in the treatment of rheumatoid arthritis, Ann. Rheum. Dis. 59 (2000) 841–849, https://doi.org/10.1136/ard.59.11.841.

[66] M.D. Wiese, A.M. Hopkins, C. King, M.D. Wechalekar, A. Lee, L. Spargo, R. Metcalf, L. McWilliams, C. Hill, L.G. Cleland, S.M. Proudman, Precision medicine with leflunomide: consideration of DHODH haplotype and plasma teriflunomide concentration can substantially modify outcomes in patients with rheumatoid arthritis, Arthritis Care Res. (2020), acr.24236, https://doi.org/10.1002/acr.24236 (Hoboken).

[67] S. Zhu, X. Yan, Z. Xiang, H.-F. Ding, H. Cui, Leflunomide reduces proliferation and induces apoptosis in neuroblastoma cells in vitro and in vivo, PLoS One 8 (2013), e71555, https://doi.org/10.1371/journal.pone.0071555.

[68] K. Hu, M. Wang, Y. Zhao, Y. Zhang, T. Wang, Z. Zheng, X. Li, S. Zeng, D. Zhao, H. Li, K. Xu, K. Lan, A small-scale medication of leflunomide as a treatment of COVID-19 in an open-label blank-controlled clinical trial, Virol. Sin. 35 (2020) 725–733, https://doi.org/10.1007/s12250-020-00258-7.

[69] H.-H. Hoffmann, A. Kunz, V.A. Simon, P. Palese, M.L. Shaw, Broad-spectrum antiviral that interferes with de novo pyrimidine biosynthesis, Proc. Natl. Acad. Sci. 108 (2011) 5777–5782, https://doi.org/10.1073/pnas.1101143108.

[70] M. Belen Cassera, Y. Zhang, K.Z. Hazleton, V.L. Schramm, Purine and pyrimidine pathways as targets in Plasmodium falciparum, Curr. Top. Med. Chem. 11 (2011) 2103–2115, https://doi.org/10.2174/156802611796575948.

[71] E. Maklashina, G. Cecchini, The quinone-binding and catalytic site of complex II, Biochim. Biophys. ActaBioenerg. 1797 (2010) 1877–1882, https://doi.org/10.1016/j.bbabio.2010.02.015.

[72] A. Mehta, C. Shaha, Apoptotic death in Leishmania donovani promastigotes in response to respiratory chain inhibition, J. Biol. Chem. 279 (2004) 11798–11813, https://doi.org/10.1074/jbc.M309341200.

[73] N. Kaila, K. Janz, S. DeBernardo, P.W. Bedard, R.T. Camphausen, S. Tam, D.H. H. Tsao, J.C. Keith, C. Nickerson-Nutter, A. Shilling, R. Young-Sciame, Q. Wang, Synthesis and biological evaluation of quinoline salicylic acids as P-selectin antagonists, J. Med. Chem. 50 (2007) 21–39, https://doi.org/10.1021/jm0602256.

[74] W. Knecht, M. Löffler, Species-related inhibition of human and rat dihydroorotate dehydrogenase by immunosuppressive isoxazol and cinchoninic acid derivatives, Biochem. Pharmacol. 56 (1998) 1259–1264, https://doi.org/10.1016/S0006-2952(98)00145-2.

[75] W. Knecht, J. Henseling, M. Löffler, Kinetics of inhibition of human and rat dihydroorotate dehydrogenase by atovaquone, lawsone derivatives, brequinar sodium and polyporic acid, Chem. Biol. Interact. 124 (2000) 61–76, https://doi.org/10.1016/S0009-2797(99)00144-1.

[76] G.C. Brandão, F.C.Rocha Missias, L.M. Arantes, L.F. Soares, K.K. Roy, R. J. Doerksen, A.Braga de Oliveira, G.R. Pereira, Antimalarial naphthoquinones. Synthesis via click chemistry, in vitro activity, docking to Pf DHODH and SAR of lapachol-based compounds, Eur. J. Med. Chem. 145 (2018) 191–205, https://doi.org/10.1016/j.ejmech.2017.12.051.

[77] R.S. Peres, G.B. Santos, N.T. Cecilio, V.A.P. Jabor, M. Niehues, B.G.S. Torres, G. Buqui, C.H.T.P. Silva, T.D. Costa, N.P. Lopes, M.C. Nonato, F.S. Ramalho, P. Louzada-Júnior, T.M. Cunha, F.Q. Cunha, F.S. Emery, J.C. Alves-Filho, Lapachol, a compound targeting pyrimidine metabolism, ameliorates experimental autoimmune arthritis, Arthritis Res. Ther. 19 (2017) 47, https://doi.org/10.1186/s13075-017-1236-x.

[78] J.M. Monteiro, P.B. Fernandes, F. Vaz, A.R. Pereira, A.C. Tavares, M.T. Ferreira, P. M. Pereira, H. Veiga, E. Kuru, M.S. VanNieuwenhze, Y.V. Brun, S.R. Filipe, M. G. Pinho, Cell shape dynamics during the staphylococcal cell cycle, Nat. Commun. 6 (2015) 8055, https://doi.org/10.1038/ncomms9055.

[79] P.D. Antonio, M. Lasalvia, G. Perna, V. Capozzi, Scale-independent roughness value of cell membranes studied by means of AFM technique, Biochim. Biophys. ActaBiomembr. 2012 (1818) 3141–3148, https://doi.org/10.1016/j.bbamem.2012.08.001.

[80] K. Seidl, S. Müller, P. François, C. Kriebitzsch, J. Schrenzel, S. Engelmann, M. Bischoff, B. Berger-Bächi, Effect of a glucose impulse on the CcpA regulon in *Staphylococcus aureus*, BMC Microbiol. 9 (2009) 95, https://doi.org/10.1186/1471-2180-9-95.

[81] G.A. Somerville, B. Saïd-Salim, J.M. Wickman, S.J. Raffel, B.N. Kreiswirth, J. M. Musser, Correlation of acetate catabolism and growth yield in *Staphylococcus aureus*: implications for host-pathogen interactions, Infect. Immun. 71 (2003) 4724–4732, https://doi.org/10.1128/IAI.71.8.4724-4732.2003.

[82] J.D. Rabinowitz, S. Enerbäck, Lactate: the ugly duckling of energy metabolism, Nat. Metab. 2 (2020) 566–571, https://doi.org/10.1038/s42255-020-0243-4.

[83] P. Geigenberger, B. Regierer, A. Nunes-Nesi, A. Leisse, E. Urbanczyk-Wochniak, F. Springer, J.T. van Dongen, J. Kossmann, A.R. Fernie, Inhibition of de novo pyrimidine synthesis in growing potato tubers leads to a compensatory stimulation of the pyrimidine salvage pathway and a subsequent increase in biosynthetic performance, Plant Cell 17 (2005) 2077–2088, https://doi.org/10.1105/tpc.105.033548.

[84] H.P. de Koning, D.J. Bridges, R.J.S. Burchmore, Purine and pyrimidine transport in pathogenic protozoa: from biology to therapy, FEMS Microbiol. Rev. 29 (2005) 987–1020, https://doi.org/10.1016/j.femsre.2005.03.004.

[85] R. Zrenner, M. Stitt, U. Sonnewald, R. Boldt, Pyrimidine and purine biosynthesis and degradation in plants, Annu. Rev. Plant Biol. 57 (2006) 805–836, https://doi.org/10.1146/annurev.arplant.57.032905.105421.